Research articles

Effect of grain size and magnetic texture on iron-loss components in NO electrical steel at different frequencies

N. Leuning*, S. Steentjes, K. Hameyer

Institute of Electrical Machines (IEM), RWTH Aachen University, D-52062 Aachen, Germany

ABSTRACT

The magnetic properties of non-grain-oriented (NO) electrical steels are a direct product of their inherent material properties in combination with induced changes due to material processing and external operational conditions such as magnetization and frequency. Chemical composition, grain size and texture are elementary intrinsic factors which determine the magnetic properties. Focus of this study is to improve the understanding of grain size and texture as important factors that affect different loss-components. A strong focus is placed on the frequency dependence and concurrent loss component distribution over application relevant frequency ranges of electrical machines. Due to its impact on the eddy current losses as well as the hysteresis components, the final thickness is additional subject of this study. A total of seven materials are produced on an experimental production line from one alloy. By different production and processing steps, different grain structures, textures and final thickness are achieved. The changes in the materials are attributed to the process variations and magnetically characterized. A loss separation procedure as well as loss modeling is performed and discussed. This work is part of a research field which aims to improve parametric models with low additional computational effort for the numerical simulation of electrical machines. The goal is to improve the accuracy of models with a deeper understanding of the material science.

1. Introduction

NO electrical steels are used to direct and concentrate the magnetic flux in rotating electrical machines. Due to extending requirements on the power density and efficiency of electrical machines, higher speed and a resulting increase of magnetization frequencies is necessary [1–3]. Speed variable traction drives for automotive applications can operate in the range of >400 Hz [4]. The loss modeling of FeSi for the design of traction drives faces the challenging reproduction of actual material behavior [5].To account for complex operation and application conditions, the basic relations for example between grain size and the loss component distribution need to be understood and modeled first. In this context, the frequency dependence of the magnetic properties of electrical steel sheets is fundamentally important. The magnetic loss of ferromagnetic materials depends on several factors. For FeSi electrical steels the primary factors are the chemical composition, the geometry, i.e., the sheet thickness, the microstructure and texture, and the mechanical residual stress within the laminations [6–10].

These contributing factors relate to different loss mechanisms which also exhibit different and in some cases, opposing frequency dependence [8,11]. As a result, basic material design relations for low

frequencies cannot be directly transferred to high frequencies. The classification of materials based on their magnetic loss at a nominal point of 1.5 T and 50 Hz in combination with the value of sheet thickness, is insufficient. The microstructure, texture and geometry on the other hand, can give indication of the relative frequency dependence of materials with similar chemical compositions and could therefore be better suited to identify applicable materials for specific requirements.

In this study, a loss separation is performed on samples that are produced on an experimental production route comprising hot rolling, cold rolling and final annealing. The processing parameters are deliberately selected to create different microstructures, textures and final thicknesses from the same alloy. The loss components are determined from quasi-static and AC-measurements up to 1000 Hz, on a single-sheet-tester (SST). A detailed evaluation of the microstructure and texture across the entire sheet thickness ensures considerations of microstructural features that account for possible inhomogeneities. The quantification of texture by means of the so-called *A*-parameter [12], enables the consideration of magnetic anisotropy and directional dependence of the magnetic loss and magnetization. The loss component distributions are evaluated at different frequencies. Two approaches at loss-modeling are conducted and compared.

---

* Corresponding author.
  E-mail address: nora.leuning@iem.rwth-aachen.de (N. Leuning).

Table 1
Chemical composition of the material under study in wt%.

Fe	C	Si	Mn	P	S	Al
balanced	0.0020	2.42	0.160	0.020	0.003	0.340

2. Experimental

In this study, different materials are produced from an alloy of 2.4 wt% FeSi by different production and processing variations. A detailed chemical composition is given in Table 1. The chemical composition corresponds to a conventional electrical steel alloy. Materials from this alloy are also industrially available in M330-50A and M300-35A quality. In order to study the effect of different grain sizes and crystallographic textures on the magnetic properties, a total of seven materials are manufactured. Process variations include hot and cold strip thickness, cold rolling reduction (CR) and final annealing temperature. In order to enable comparison between the materials, the processing parameters are selected so, as to deliver a large number of final materials by combination of just limited variations in each processing step. From two different hot strip thicknesses, two final thicknesses are cold rolled, resulting in three distinct cold CRs of 50%, 75% and 80%. The hot strip is produced from a 64-mm continuously cast thin slab feedstock on a four-stand semi-continuous hot-rolling mill.The hot rolling start temperature was 1180 °C after reheating the slab and then soaking it for 60 min at 1220 °C. Exit temperature and coiling were conducted by 890 °C and 800 °C respectively. Cold rolling is performed to achieve a final thickness of 0.5 mm and 0.25 mm of the final steel strips. The annealing temperatures of 900 °C, 1000 °C and 1200 °C are chosen in order to achieve large differences in grain size with the premise of a fully recrystallized microstructure, which has been ensured with additional annealing experiments. In Table 2 the processing parameters for the seven materials are summarized. The production processes are executed in industry relevant parameter ranges. However, the laboratory scale differs from the industrial process due to continuity, for example on the annealing (continous vs. batch annealing), strip forces during the rolling and coiling and overall batch size.

Analysis of grain size and texture is obtained by evaluation and characterization in different layers across the sheet thickness of the produced materials. As previously established two to three layers of the rolling direction (RD)-transverse direction (TD) plane depending on the sheet thickness d_{sheet} are prepared, as displayed in Fig. 1, to account for possible inhomogeneities of grain size and texture across the sheet thickness [13]. The metallographic macro texture is measured via X-ray diffraction and the texture is calculated by an automated goniometer tool. In this paper the orientation distribution function (ODF) is used to calculate the A-parameter using an approach by [12]. The parameter is an indicator for the magnetization behavior on basis of the crystallographic orientation. Due to the magnetic anisotropy of the FeSi single crystals with easiest magnetization along the ⟨100⟩-directions (cube edges), inferior magnetization along the ⟨110⟩-direction (surface diagonals) and hardest magnetization along the ⟨111⟩-directions (room diagonal) the magnetic properties depend on the crystallographic texture [14]. In this context, the A-parameter describes an angle, which is the

Table 2
Production and processing of the seven different materials with hot (d_{HS}) and cold strip thickness (d_{CS}), annealing temperature (T_a) and cold rolling reduction (CR).

	#1	#2	#3	#4	#5	#6	#7
d_{HS}	1.0 mm	1.0 mm	1.0 mm	1.0 mm	1.0 mm	2.4 mm	2.4 mm
CR	50 %	50 %	75 %	75 %	75 %	80 %	80 %
d_{CS}	0.5 mm	0.5 mm	0.25 mm	0.25 mm	0.25 mm	0.5 mm	0.5 mm
T_A	1000 °C	1200 °C	900 °C	1000 °C	1200 °C	1000 °C	1200 °C

mean of the smallest angles between the easy magnetization ⟨100⟩-directions of the entirety of intensities of an ODF, characterized by their Euler-angles and the magnetization vector. Consequently, a smaller angle indicates easier magnetization in a specific direction. For this study the A-parameters are calculated for RD and TD, which are the directions that are analyzed magnetically. Grain size is also determined in different layers on light microscopy images. Grain boundary etching is performed by using a 5% Nital solution. The line-intercept method is applied to determine the mean grain length in RD and TD direction. With this method a set of parallel line segments are placed on the micrograph, and the numbers of times each line segment intercepts a grain boundary is counted, the ratio to the length of the line gives a mean value of the grain size. A minimum of 300 grains are measured for each sample in both directions RD and TD.

Magnetic measurements are performed on a 60 mm × 60 mm SST from Brockhaus measurement systems. The *J-H*-characteristics at polarizations between 0.3 T and 1.8 T are measured under quasi-static excitations and under sinusoidal magnetic flux excitation of frequencies of 10 Hz, 50 Hz, 100 Hz, 400 Hz and 1000 Hz.

3. Results

3.1. Microstructure and texture

In this section results of the microstructure and texture for the produced materials are presented. In order to incorporate possible homogeneities across the sheet thickness, the grain size as well as the A-parameter are weighted for the different layers across the sheet thickness according to the following Eqs. (1) and (2).

$$d_{GS} = \frac{d_{GS0\%} + 2 \cdot d_{GS25\%} + d_{GS50\%}}{4} \tag{1}$$

$$A_\theta = \frac{A_{\theta0\%} + 2 \cdot A_{\theta25\%} + A_{\theta50\%}}{4} \tag{2}$$

From the results displayed in Fig. 2 and Table 3 it is evident that the annealing temperature has a dominant effect on grain growth, whereas the CR has a minor effect. Grain size for low temperature annealing (900 °C) are below 40 μm. For the 1000 °C annealing temperatures, grain sizes are between 45 μm and 65 μm. For the 1200 °C annealing, grain sizes are scattered over a wide range from 160 μm for material #5 to 340 μm for material #7. It is likely that grain growth is affected when grains become in a range of the size of the sheet thickness. Further growth is impeded, which leads to smaller grains in the 0.25-mm sheets. But also material #2 and #7 have distinct differences in grain size which leads to the assumption that also the hot strip or CR affect grain evolution during final annealing. In total grains have nearly spherical dimension. Some differences between grain sizes in RD and TD occur, but they do not exceed 8%. Additionally there is no distinct relation between grain size anisotropy and sample direction observed. For the crystallographic texture on the other hand, results show a clear anisotropy. Though the texture is not a sharp texture, from the results of the calculated A-parameter, magnetic properties in RD are likely to be better than in TD, because, more easy magnetization directions are aligned closer to RD, as displayed in Table 4. The best possible texture for NO electrical steel laminations is a rotated-cube fiber, which comprises an even distribution of ⟨100⟩ directions within the RD-TD-plane. An even distribution increases the isotropy in the sheet plane and contributes to a homogeneous magnetic field during application. This fiber orientation has a value of 22.5 whereas the γ-fiber with the largest amount of ⟨111⟩-room diagonals in the sheet plane is expected to have the most detrimental effect on the magnetic properties for NO, with an A-parameter of 38.7 [12,9].
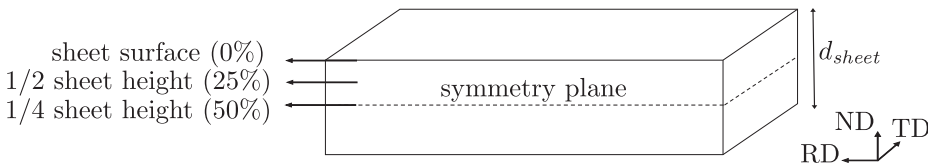
sheet surface (0%)
1/2 sheet height (25%)
1/4 sheet height (50%)

symmetry plane

d_{sheet}

ND TD
RD

Fig. 1. Schematic illustration of sample preparation for microstructural analysis in different layers of the RD-TD-plane, according to [13].

3.2. Loss separation

The loss separation is performed according to the Bertotti loss theory (3) [15], where the measured magnetic loss P_s at different frequencies is separated into its hysteresis P_{hyst}, classical eddy current P_{cl} and excess loss P_{exc} components.

$$P_s = P_{hyst} + P_{cl} + P_{exc} \tag{3}$$

The hysteresis loss component P_{hyst} is calculated from DC-measurements. With a linear relation to the frequency f the hysteresis

Table 3
Mean grain diameters d_{GS} for material #1 to #7, (#1) 50% CR, 1000 °C, (#2) 50% CR, 1200 °C, (#3) 75% CR, 900 °C, (#4) 75% CR, 1000 °C, (#5) 75% CR, 1200 °C, (#6) 80% CR, 1000 °C, (#7) 80% CR, 1200 °C.

d_{GS}	#1	#2	#3	#4	#5	#6	#7
RD	48 μm	241 μm	36 μm	63 μm	162 μm	55 μm	340 μm
TD	51 μm	228 μm	36 μm	63 μm	168 μm	58 μm	313 μm

a) #1

b) #2

c) #3

d) #4

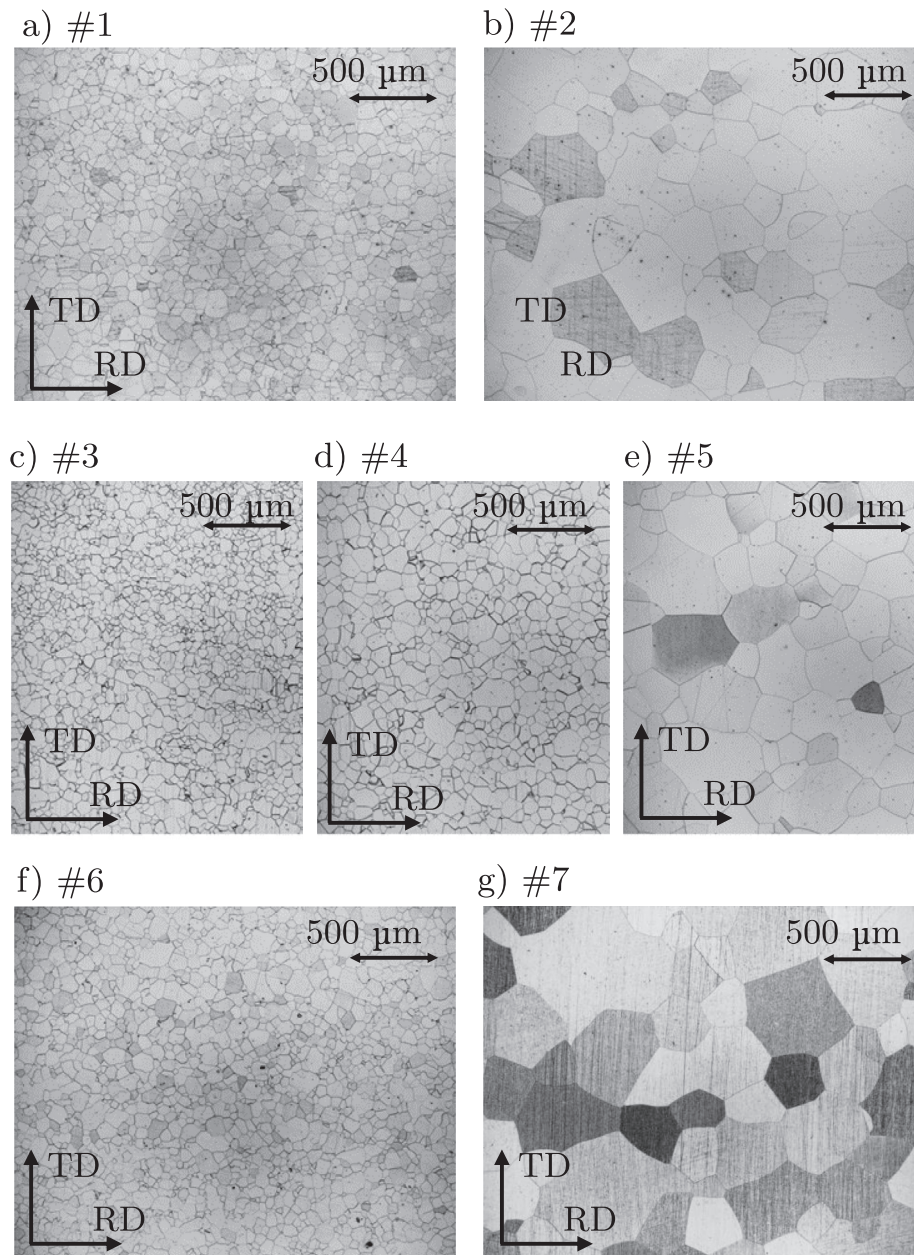
e) #5

f) #6

g) #7

Fig. 2. Ligh optical microscopes for material 1–7, (a) 50% CR, 1000 °, (b) 50% CR, 1200 °, (c) 75% CR, 900 °, (d) 75% CR, 1000 °, (e) 75% CR, 1200 °, (f) 80% CR, 1000 °, (g) 80% CR, 1200 °.

Table 4

Mean A-parameters for material #1 to #7, (#1) 50% CR, 1000 °C, (#2) 50% CR, 1200 °C, (#3) 75% CR, 900 °C, (#4) 75% CR, 1000 °C, (#5) 75% CR, 1200 °C, (#6) 80% CR, 1000 °C, (#7) 80% CR, 1200 °C.

A_ϑ	#1	#2	#3	#4	#5	#6	#7
RD	30.77	29.55	30.17	30.09	28.04	29.84	28.77
TD	34.72	33.63	33.32	33.60	32.27	33.08	31.06

Table 5

Magnetic loss at 1.5 T and 50 Hz for samples #3 to #5 in RD and TD and theoretical classification.

	$P_{s,\ RD}$	$P_{s,\ TD}$	$P_{mean\ RD,TD}$	classification
#3	4.81	5.14	4.97	M500-25A
#4	3.30	3.75	3.53	M360-25A
#5	2.80	3.07	2.93	M300-25A

component is determined for each frequency up to 1000 Hz. The classical eddy current loss component P_{cl} is calculated solely from physical parameters as displayed in Eq. (4). Here, the peak induction $\widehat{B}$, sheet thickness d_{sheet}, frequency f, material density ρ, and electrical resistivity ρ_{el} are used to determine the contribution of classical eddy current loss.

$$P_{cl} = \frac{(\pi \cdot \widehat{B} \cdot f \cdot d_{sheet})^2}{6 \cdot \rho \cdot \rho_{el}} \qquad (4)$$

With the classical and hysteresis loss components quantified, the excess loss is determined by subtraction of these components from the measured magnetic loss P_s at the given frequencies. Eq. (5) summarizes the approach. The loss separation is performed in RD as well as TD.

$$P_{exc} = P_s \overset{meas.}{\nearrow} - P_{hyst} \overset{DC\text{-}meas.}{\nearrow} - P_{cl} \overset{calc.\ (4)}{\nearrow} \qquad (5)$$

Eq. (5) has shown to be inaccurate [16]. The use of numerical models as presented in [17] can increase the accuracy. In Section 3.4 a numerical approach for the determination of eddy current losses is presented and compared to the results obtained by Eq. (4). For the materials under study, the accuracy of the Bertotti approach is sufficient for the loss separation and correlation to microstructural parameters.

In Fig. 3 results of the loss separation are displayed for samples with
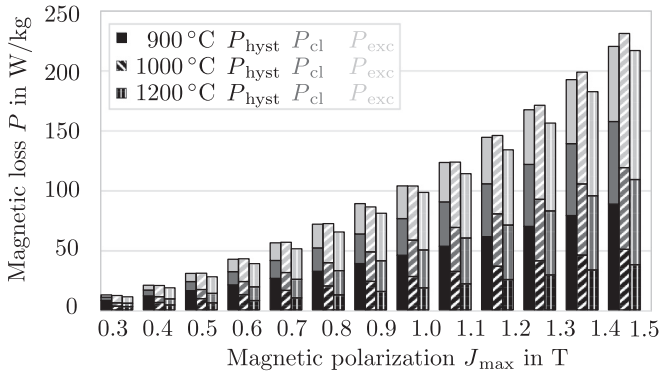
a) 50 Hz, RD
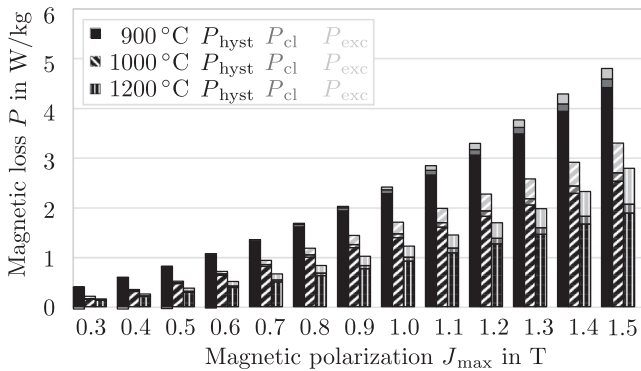
b) 1000 Hz, RD

Fig. 3. Loss separation according to Eq. (5) for samples with 0.25 mm final thickness, #3 (75% CR, 900 °C), #4 (75% CR, 1000 °C), #5 (50% CR, 1200 °C) at, (a) 50 Hz and (b) 1000 Hz.

a final thickness of 0.25 mm. The three materials' processing only differ by the final annealing temperature. At 50 Hz there is a strong dominance of the hysteresis loss component, which therefore prevail on the overall magnetic loss at low frequencies. Due to the same alloying concept, especially the Si and Al content which affects the electrical resistivity ρ_{el} and only microns difference in final thickness the classical eddy current loss is almost identical for the three samples displayed. The excess loss shows a behavior contrary to the hysteresis loss, but constitutes to the overall loss only to a small extend. In Fig. 3 the results are displayed for measurements in RD. The results in TD show the exact tendencies that were just summarized with slightly inferior magnetic properties. A mean from RD and TD is generally used to classify the materials based on their nominal loss at 1.5 T and 50 Hz. In Table 5, a theoretical classification based on the following norm EN 10106:2007 is displayed. From this classification #5 is by far the highest steel grade. However, this evaluation is only valid for low frequency applications. At increasing frequencies this classification is insufficient. The distribution of loss components changes and the excess loss component has a stronger effect on total loss than the hysteresis loss component. The overall loss for #3 at 1000 Hz is now smaller than for #4. However, #5 still has the smallest loss. For the other samples with 0.5-mm thickness, i.e., #1, #2 and #6, #7, this change is even more pronounced. As displayed in Fig. 4 for #6 and #7 (80% CR), the samples with the highest annealing temperature are not the same samples as the ones with lowest loss at 1000 Hz, though the tendencies at low frequencies are as expected, i.e., a strong relation between high annealing temperatures and low loss. For the 50% CR the behavior at high frequencies is additionally polarization dependent. At low and high polarizations the higher annealed (1200 °C) samples exhibit greater loss whereas at medium frequencies the lower annealed samples (1000 °C) exhibit slightly larger loss.

The overall loss at a specific frequency depends on the distribution of loss components. In Fig. 5 the loss distribution for different frequencies and polarizations is shown exemplary for sample #1. The general relations meet the expectations. The share of hysteresis on total loss decreases with increasing polarization and frequency, whereas the amount of excess and classical loss increases.

In literature, there are various approaches to estimate the loss and according to these, the components exhibit the following frequency and polarization dependence [15,18–21]

- $P_{hyst} \sim \widehat{B}^{1.6\ldots2}, f$
- $P_{cl} \sim \widehat{B}^2, f^2$
- $P_{exc} \sim \widehat{B}^{1.5}, f^{1.5}$

The different loss components can be attributed to different structural features of the material [20,11]. If these relations are quantified and the loss distributions can be estimated with existing loss models, the operating relevant structural parameters for electrical steel sheets can be identified and used to chose materials for specific applications frequencies.

3.3. Correlation of microstructure and loss components

The results of the loss separation in Section 3.2 can now be attributed to the microstructural features of the material under study of
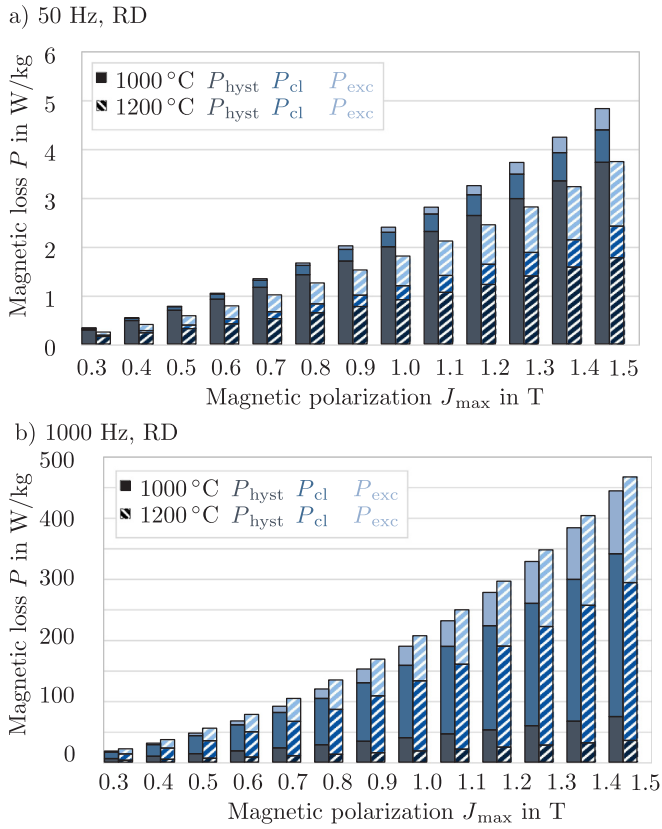
a) 50 Hz, RD

b) 1000 Hz, RD

Fig. 4. Loss separation according to Eq. (5) for samples with 0.5 mm final thickness, #6 (80% CR, 1000 °C), #7 (80% CR, 1200 °C) at, (a) 50 Hz and (b) 1000 Hz.
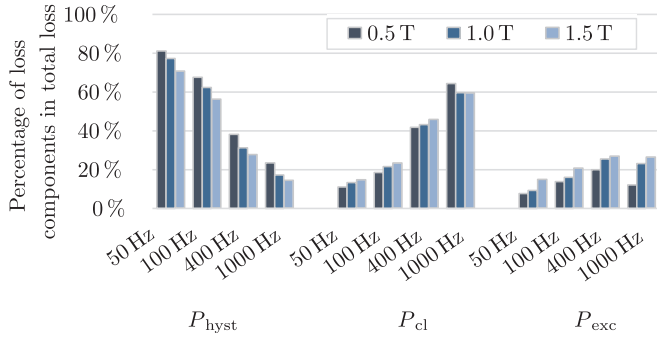

Fig. 5. Distribution of loss components st different frequencies and polarizations for material #1 (50% CR, 1000 °C).
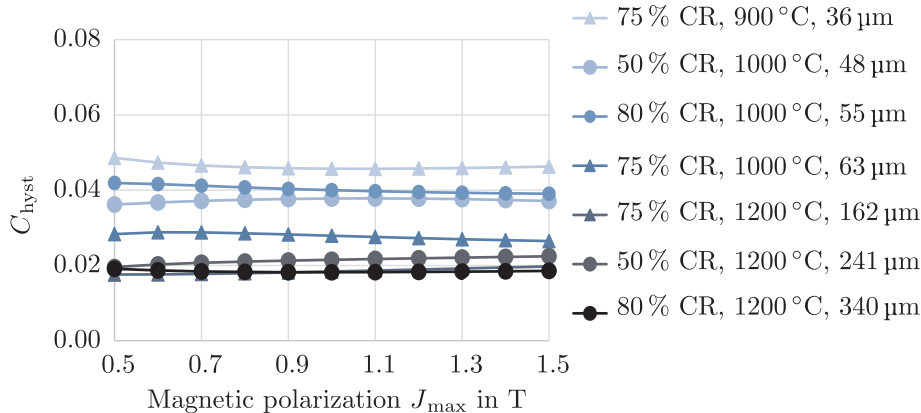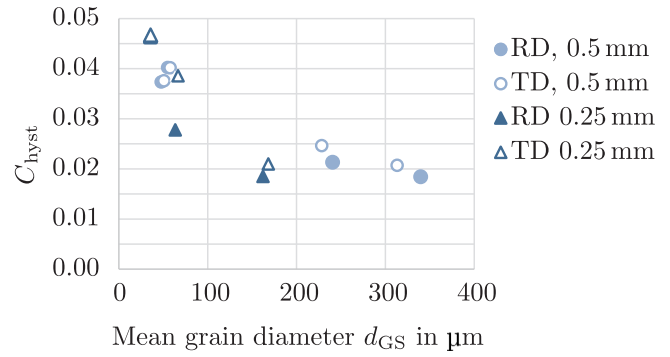

Fig. 7. Dependence of C_{hyst} determined by Eq. (6) and averaged between 0.5 T and 1.5 T for samples in RD and TD on grain size.

Section 3.1. Due to the same alloying for all samples and only slight variations of processing the overlap of the materials is sufficient to attribute changes for loss and magnetization to the changes between the materials, i.e., thickness, grain size and texture.

Grain size has an especially strong effect on different loss components, as stated in various research to which the presented results are corresponding. The texture on the other hand has a minor effect in this study. Texture measurements show that due to the NO behavior of the samples, the difference in texture between the different materials is relatively small. Although, the anisotropy is affected by microstructure, which will be discussed in Section 3.5, the difference in materials is not dominantly affected, i.e., texture in RD is always magnetically favorable compared with TD. This estimation is based on the amount of easy magnetization axes closer to RD direction. Therefore, the following results are mainly compared between samples in only one spatial direction.

The hysteresis loss decreases with increasing grain size (see Fig. 6). This can be deduced from the results displayed so far. Thus, higher annealing temperatures lead to larger grains and lower hysteresis loss. Considering, P_{hyst} is proportional to f and $B^{1.6\ ...2.0}$ a factor C_{hyst} can be determined. The frequency dependence is linear. In order for C_{hyst} to be a factor instead of a function, the B dependency is set to the power of 1.6 for the studied samples, according to Eq. (6).

$$C_{hyst} = \frac{P_{hyst}}{f \cdot \widehat{B}^{1.6}} \tag{6}$$

The results for the determined C_{hyst} in RD are depicted in Figs. 6 and 7. Two structural material parameters correlate with this factor and are emphasized by graphical measures in Fig. 6. Sheet thickness is highlighted by different marker styles, i.e., round markers for 0.5 mm sheets and triangular markers for 0.25 mm sheets and a color gradient from light to dark for increasing grain size. It is observed that the hysteresis
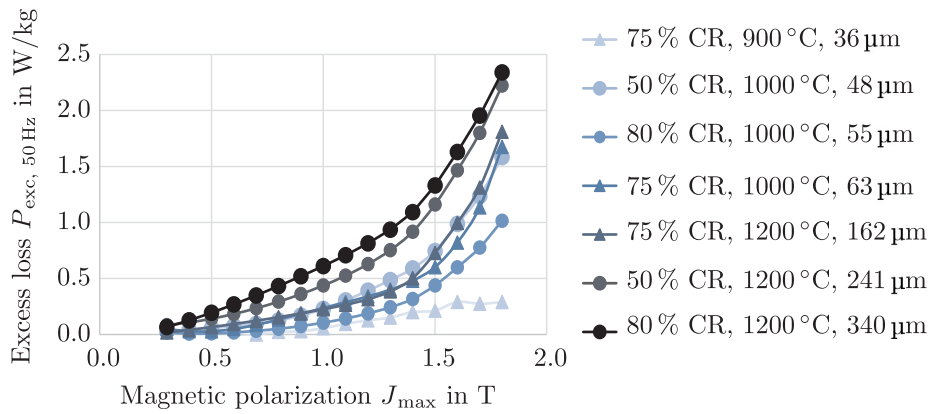

Fig. 6. C_{hyst} determined by Eq. (6) between 0.5 T and 1.5 T for samples in RD, with consideration of grain size.

Fig. 8. Excess-loss P_{exc} at 50 Hz for samples #1 to #7 in RD with consideration of grain size.
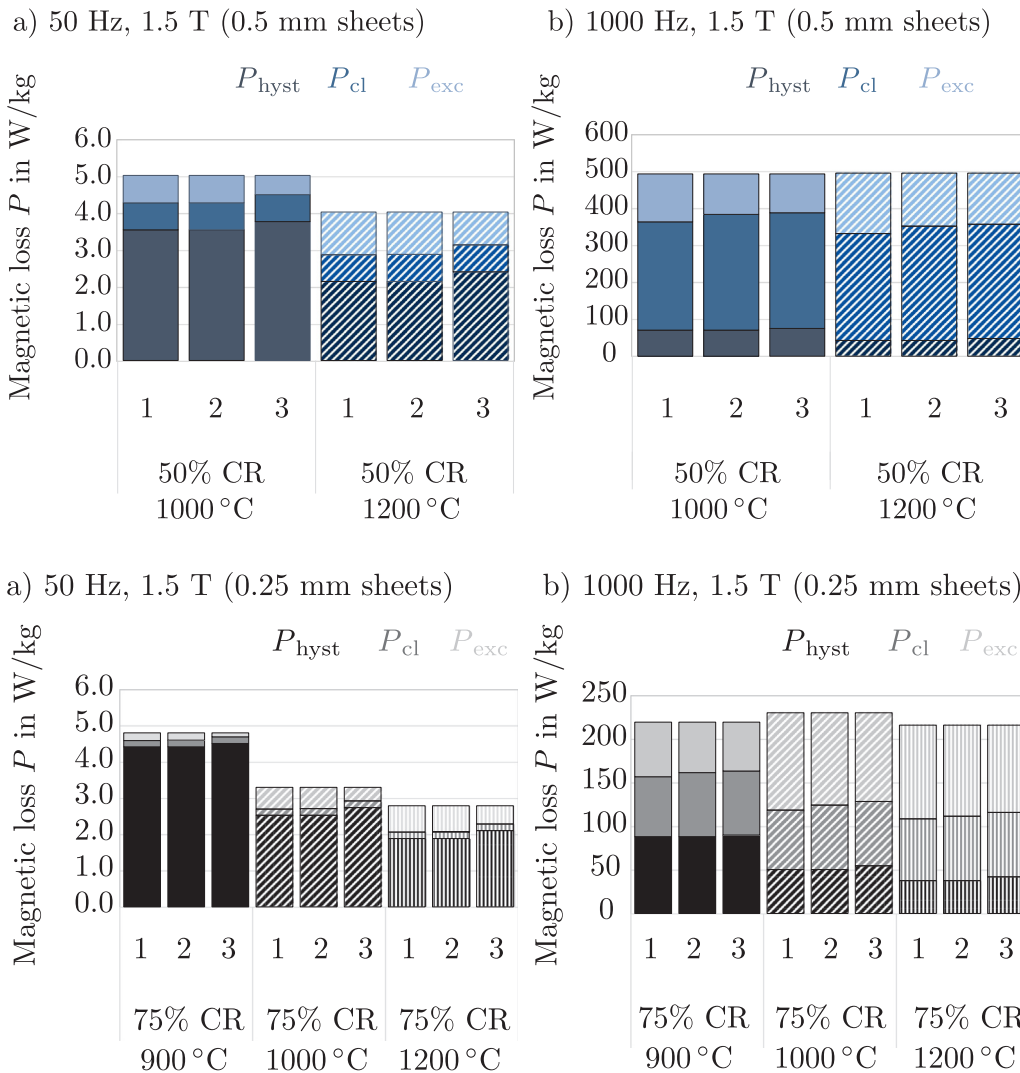

Fig. 9. Distribution of loss components at 1.5 T and (a) 50Hz an (b) 1000 Hz. 1: Loss separation according to Section 3.2 with P_{cl} determined by Eq. (4), 2: Loss separation according to Section 3.2 P_{cl} simulated, 3: Loss separation according to Section 3.2 P_{cl} simulated and P_{hyst} estimated from 10 Hz measurements instead of DC measurements.

Fig. 10. Distribution of loss components at 1.5 T and (a) 50 Hz an (b) 1000 Hz. 1: Loss separation according to Section 3.2 with P_{cl} determined by Eq. (4), 2: Loss separation according to Section 3.2 P_{cl} simulated, 3: Loss separation according to Section 3.2 P_{cl} simulated and P_{hyst} estimated from 10 Hz measurements instead of DC measurements.

loss factor decreases with grain size as well as with sheet thickness, which is in accordance with various research [22,23,11]. There is however one exception from this behavior for the samples with 0.5 mm final thickness and 1000 °C annealing. Here, the smaller grains with 48 μm lead to a smaller C_{hyst} compared to 55μm. There are possible reasons for this deviation. The first is the contribution of mechanical stress to the hysteresis loss component. Mechanical stress has a significant effect on the hysteresis loss component [24,25]. Compressive

stress deteriorates the magnetic properties significantly, whereas the effect of tensile stress is more divergent [26]. The produced samples can have different mechanical residual stress due to their difference in processing. Different rolling and annealing strategies affect the stress state. Another reason for the differences can be due to the method of grain size determination. Grain sizes are determined by line intercept method, where the distances between grain boundaries on horizontal measurement lines is averaged. The distribution of grain sizes can
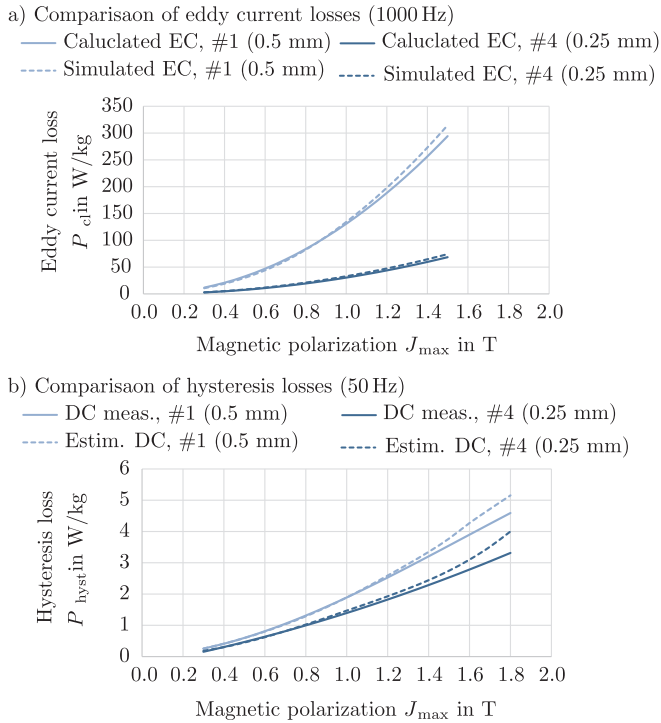
Fig. 11. Comparison of (a) simulated and calculated eddy current (EC) loss and (b) of hysreresis loss from DC meausrements and estimated from 10 Hz for samples #1 and #4.

however, differ significantly, with some materials exhibiting homogeneous grain sizes and others exhibiting selective grain growth, i.e., large grains surrounded by smaller grains. Nevertheless, the general trend between grain size and C_{hyst} can be denoted for samples both in RD and TD.

In Fig. 7 C_{hyst} of samples both in RD and TD are displayed as a function of grain size. For small grain sizes C_{hyst} decreases but approximates a plateau where an increase of grain size does not lead to further decrease of C_{hyst}. In this figure the different slopes for the thicknesses can also be noticed.

The observations on the contradicting tendencies of hysteresis and excess loss from the previous Section 3.2 with Figs. 3 and 4 can be transferred from annealing temperatures to grain size. Larger grain sizes lead to higher excess losses and smaller hysteresis losses. This is also observed in literature and displayed in Fig. 8. The excess losses are depicted at 50 Hz. The trend of decreasing excess loss with smaller grain size is distinct. A dependency of thickness cannot be observed. Unusual behavior regarding the polarization dependence is observed for the 900 °C annealed samples, with only a relatively small polarization dependence. Furthermore, samples with 50% CR show very high losses that cannot be attributed solely to grain size variation.

3.4. Loss modeling

An easy parametric model for the calculation of iron losses in electrical machines can be modeled after the Bertotti loss model (7) [15].

$$P_{Bertotti} = P_{hyst}\widehat{B}^2 f + P_{cl}\widehat{B}^2 f^2 + +P_{exc}(\widehat{B}f)^{1.5} \tag{7}$$

The strength of the Bertotti model is its comprehensive physical explanation, as discussed in Section 3.2 and 3.3. However, it has a weakness in the estimation of loss at high frequencies and inductions. In [27,28] it is shown that the classical Bertotti model often underestimates losses at high magnetic flux densities and high frequencies.In [27] the IEM Formula is introduced, which takes the Bertotti model but

adds an additional term, called saturation loss to the loss equation to account for non-linear material behavior. This results in the mathematical formulation (8). The IEM-Formula shows improvement in loss determination at high magnetic flux densities and high frequencies, due to this fourth loss term with a higher order $\widehat{B}$ dependence [29].

$$P_{IEM} = a_1\widehat{B}^{\alpha+\widehat{B}\beta}f + a_2\widehat{B}^2f^2 + a_2a_3\widehat{B}^{2+a_4}f^2 + a_5(\widehat{B}f)^{1.5} \tag{8}$$

As previously discussed, the modeling of the eddy loss component is subject of controversy. Research suggests that the accuracy can be improved by numerical simulation of eddy currents [16,17]. The computational effort thereby increases. As the authors of [16] note, the simplified loss prediction routines, as presented here can still an acceptable approximation for loss modeling. In order to determine if the use of Eq. (4) is sufficient for the Bertotti and IEM formula and the materials under study, a comparison has been conducted.

For that purpose the Maxwell diffusion equation is solved by using the meshfree model described in [30]. Neglecting edge effects the problem is reduced to the integration of a 1-D penetration equation that links the magnitudes of the magnetic field strength *H*, the magnetic flux density *B*, and the electric field strength E within a material with specific electrical conductivity and a non-linear *B(H)*. In order to calculate the eddy-current losses, the anhysteretic magnetization curve is used to describe the constitutive relation [31]. As a result the classical eddy-current losses for the different materials and operation conditions were obtained.

In Figs. 9 and 10 the results of a comparison between the original approach for loss separation of section 3.2 is compared to a loss separation in which the eddy current losses are simulated and an approach where the classical eddy current losses are simulated and DC losses are estimated from 10 Hz measurements instead of point-point DC measurements. The results show that for cases 1 and 2, neither the eddy current losses, nor the relative distribution changes for the excitation condition 1.5 T and 50 Hz and 1000 Hz respectively. The estimated DC losses are higher when they are estimated from 10 Hz measurements compared with point-to-point DC measurements. In Fig. 11 the calculated versus simulated eddy current losses are displayed for one 0.5 mm sample and one 0.25 mm sample. The relative error at 1.5 T 7% for sample #1 and 8% for sample #4. For the DC estimation the relative errors at 1.5 T are 6% both, for sample for sample #4. As previously mentioned the loss distribution is not significantly affected by this difference.

The Bertotti and the IEM models are used to model the loss of the materials and the results are compared (see Fig. 12).The identification methods for C_{hyst}, C_{cl} and C_{exc} for the Bertotti model, as well as a_i, α and β for the IEM formula are described in [18,29]. In Fig. 3.5 results are displayed for the 0.25 mm samples at 50 Hz and 1000 Hz. For both models and the studied materials, there is no parameter set leads to sufficient accuracy at both low and high frequencies. Considering the models at 50 Hz, the fit for the 900 °C annealed samples is good for both models with a mean error over the entire polarization range of <3%. At 1000 °C both models have an offset at high polarizations. The trend of the error is almost identical with a relative error at 1.6 T 7% and 8%, at 1.7 T of 12% and 13% and at 1.8 T of 20% and 23%. For the 1200 °C the models behave differently. The slope of the curve is better portrayed by the IEM formula but the overall error is still pronounced, especially at high polarizations. At 50 Hz the fit appears to depend somehow on the microstructure, with a good fit for the smaller grain size and worse fit for coarser grains, i.e., for higher temperature as annealed samples. Especially the different shape of the curves for the materials are not portrayed correctly. At 1000 Hz the relative error for both models is more random, with the models sometimes underestimating and sometimes overestimating the losses. This again is somehow related to the slope of the measurement curve, that both models don't portray exact. The results show that iron-loss models need to be improved to enhance their accuracy.With statistical identification of parameters with a larger
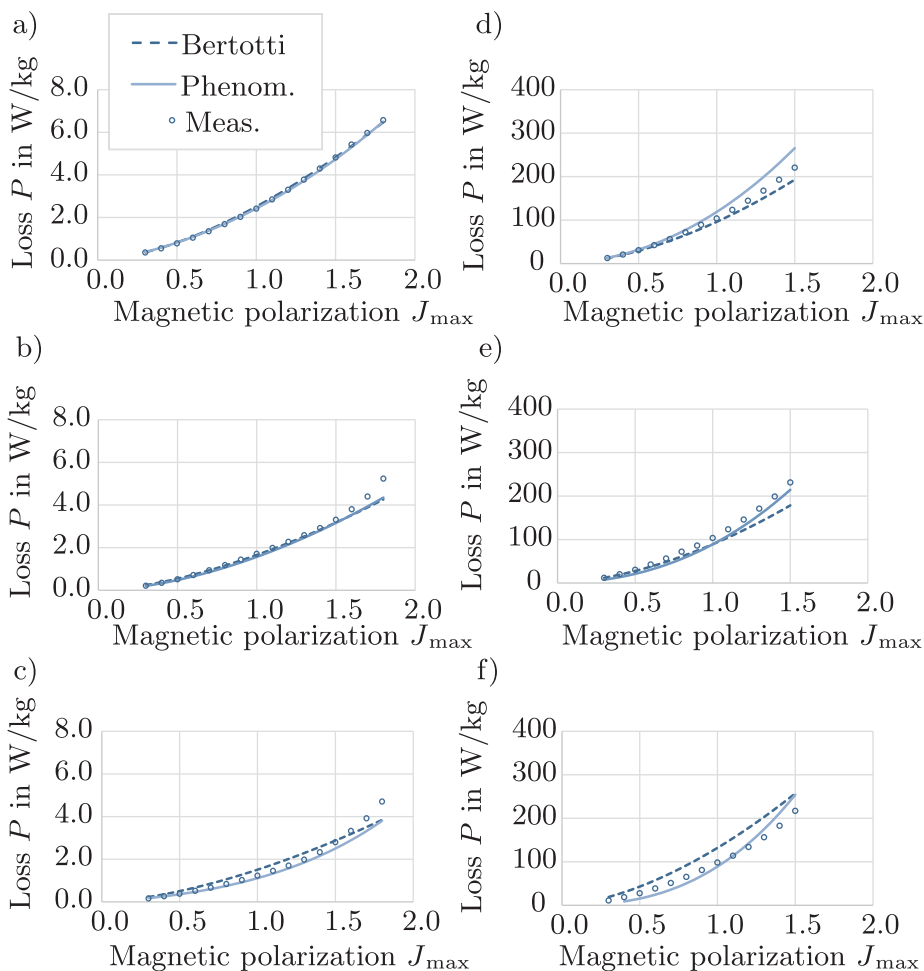
Fig. 12. Comparison of modeled and measured magnetic loss at 50 Hz and 1000 Hz, for the 0.25 mm (75% CR) samples (a) 900 °C at 50 Hz, (b) 1000 °C at 50 Hz, (c) 1200 °C at 50 Hz, (d) 900 °C at 1000 Hz, (e) 1000 °C at 1000 Hz, (f) 1200 °C at 1000 Hz.
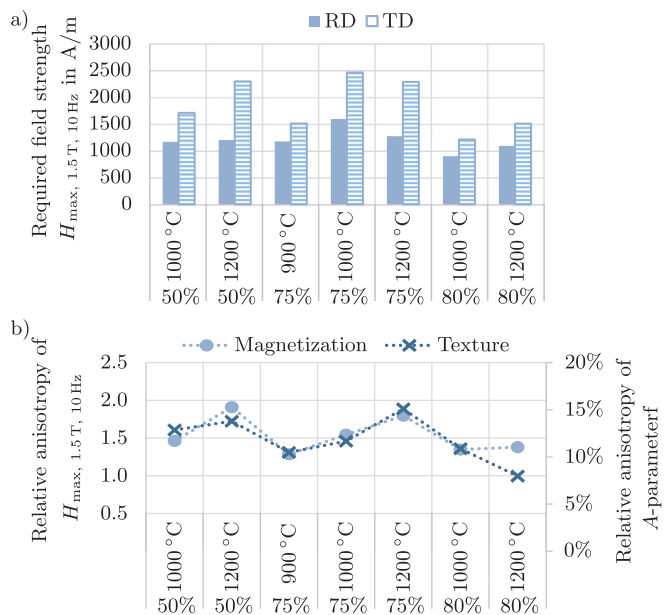

Fig. 13. (a) Magnetic anisotropy of required magnetic field strength at 1.5 T and 10 Hz and (b) relative anisotropy of A-parameter and required magnetic field strength.

number of samples with even more annealing temperatures and adaption of the model terms, the accuracy might increase. Thereby an insight to the role of grain structure on the loss components and shape of the curves can be determined.

3.5. Magnetic anisotropy

The magnetic anisotropy in this study, is characterized by comparison of magnetic properties in RD and TD and evaluation of the relative change. In full saturation, the magnetic flux density B_s is only affected by chemical composition [14,6,32]. Thus, for all produced sample sets B_s is the same. At high polarizations, where domain rotation is characteristic for the magnetization process, the influence of texture is large [11]. This is due to the magneto-crystalline anisotropy of the body-centered-cubic iron lattice. Magnetization is easiest along the cube edges compared to slightly inferior magnetization along the face diagonal and worst magnetization along the room diagonals [14]. Consequently the orientation of all grains of the polycristalline FeSi contributes to the magnetic properties and especially the anisotropy. Though the classification of NO suggests isotropic texture the production and processing still leads to certain characteristic texture components as already discussed in Section 3.1. Though, the grain size as well as mechanical stress affect the shape of the magnetization curves, they have a greater effect at low to medium polarizations [11]. In [13] the A-parameter calculated from the ODF is shown to be in good accordance with magnetic measurements of different industrial NO electrical steels at high polarizations.

In Fig. 13(a) the required magnetic field strength is displayed for all samples in RD and TD. In (b) of the same figure the relative magnetic anisotropy is displayed alongside the anisotropy of the *A*-parameter. It shows that the tendencies are very similar for this alloy leading to the assumption that the anisotropy at high polarization is actually determined by texture and that because of a rather uniform grain size that the mechanical stress is not vastly different in the different directions.

4. Conclusions

In the presented paper the effect of grain size, texture and sheet thickness as central structural material parameters on loss components and magnetization is studied, with a focus on frequency dependence. The chemical composition, although a dominant factor, has not been considered in this study, where the produced materials come from the same alloy. Seven materials have been produced on a laboratory scale processing route. Below, the key results with respect to the loss component distribution at different frequencies and the loss modeling are summarized.

- Distribution of loss components: The dependence of relevant structural parameters for the application of electrical steel on frequency arises from the distribution of loss components at different frequencies and polarization ranges. Grain size, texture and thickness affect different loss components and polarization ranges. At low frequencies P_{hyst} is dominant but increases linear with f, whereas P_{cl} and P_{exc} have a frequency dependence of higher order. The loss distribution depends on the structural parameters. Higher thickness leads to a larger share of classical eddy current loss on total loss and therefore a smaller impact of grain size.
- Grain size: With increasing grain size the hysteresis loss decreases and excess loss increases. Thus, an optimum grain size, which is dependent on frequency, exists. With variation of the annealing temperature the grain size can be altered. The interaction between grain growth and CR has to be considered. Small sheet thicknesses impede the grain growth. For low to medium frequencies up to 400 Hz larger grain sizes are favorable. At increasing frequency, i.e., 1000 Hz, smaller grains lead to equally good results as larger grains. Due to the increasing proportion of excess loss compared with hysteresis loss, smaller grains become beneficial. This means that the optimum grain size depends on the application frequency due to the ratio of excess to hysteresis loss. Smaller grains lead to higher hysteresis loss and equals a lower steel grade. Economically, lower grades are favorable. However, the interrelation with further processing, e.g., punching has to be accounted for in further considerations.
- Sheet thickness: The sheet thickness d_{sheet} of the electrical steel laminations is the dominant aspect for the frequency dependence. A thickness reduction is the easiest way to reduce core loss. At low frequencies, the interdependence with grain growth has to be accounted for. Grain growth is impeded at small sheet thickness, so that at the same annealing temperature of 1200 °C, the smaller thickness leads to distinctly smaller grains. This has an effect on hysteresis loss. Considering the loss component distribution, due to the smaller thickness, the classical eddy current loss component has a less dominant contribution to overall loss for smaller thicknesses, so that the grain size influence increases.
- Texture: In this study the texture has an inferior role for the loss components due to the small differences between the resulting textures of the differently produced materials. Still, the RD and TD anisotropy of the magnetization can be correlated to the texture for each sample.
- Loss modeling: The iron-loss models need to be improved to enhance accuracy. The aim is to improve them by means of a thorough understanding of the material science. At low frequencies the fit appears to depend somehow on the microstructure, with a good fit for

fine grains and worse fit for coarser grains, i.e. higher annealing temperatures. Especially the different shape of the curves for the materials are not portrayed correctly. A statistical identification of parameters with a larger number of samples and adaption of parameter identification might increase accuracy and give insight to the role of grain structure on the loss components and shape of the curves. Considering loss modeling, the accuracy still needs to be improved.

References

[1] D. Gerada, A. Mebarki, N.L. Brown, C. Gerada, A. Cavagnino, A. Boglietti, High-speed electrical machines: technologies, trends, and developments, IEEE Trans. Ind. Electron. 61 (6) (2014) 2946–2959, https://doi.org/10.1109/TIE.2013.2286777.
[2] L. Vandenbossche, S. Jacobs, D.V. Hoecke, B. Weber, E. Leunis, A. Attrazic, Improved iron loss modelling approach for advanced electrical steels operating at high frequencies and high inductions in automotive machines, in: 2012 2nd International Electric Drives Production Conference (EDPC), pp. 1–8. doi:10.1109/EDPC.2012.6425108.
[3] A. Ruf, S. Steentjes, G. von Pfingsten, T. Grosse, K. Hameyer, Requirements on Soft Magnetic Materials for Electric Traction Motors, in: Conf. Proc. 7th international Conference on Magnetism and Metallurgy, WMM'16, Rome, Italy, 2016, pp. 111–128.
[4] S. Steentjes, G. von Pfingsten, M. Hombitzer, K. Hameyer, Iron-loss model with consideration of minor loops applied to FE-simulations of electrical machines, IEEE Trans. Magn. 49 (7) (2013) 3945–3948, https://doi.org/10.1109/TMAG.2013.2244072.
[5] G. von Pfingsten, S. Steentjes, K. Hameyer, Operating point resolved loss calculation approach in saturated induction machines, IEEE Trans. Industr. Electron. 64 (3) (2017) 2538–2546, https://doi.org/10.1109/TIE.2016.2597761.
[6] M.F. Littmann, Iron and silicon-iron alloys, IEEE Trans. Magnetics 7 (1) (1971) 48–60, https://doi.org/10.1109/TMAG.1971.1066998.
[7] P. Brissonneau, Non-oriented electrical sheets, J. Magn. Magn. Mater. 41 (1) (1984) 38–46, https://doi.org/10.1016/0304-8853(84)90132-X.
[8] G. Bertotti, Connection between microstructure and magnetic properties of soft magnetic materials, J. Magn. Magn. Mater. 320 (20) (2008) 2436–2442, https://doi.org/10.1016/j.jmmm.2008.04.001.
[9] E. Gomes, J. Schneider, K. Verbeken, J. Barros, Y. Houbaert, Correlation between microstructure, texture, and magnetic induction in nonoriented electrical steels, IEEE Trans. Magn. 46 (2) (2010) 310–313, https://doi.org/10.1109/TMAG.2009.2032425.
[10] A. Schoppa, J. Schneider, C.D. Wuppermann, Influence of the manufacturing process on the magnetic properties of non-oriented electrical steels, J. Magn. Magn. Mater 215–216 (2000) 74–78, https://doi.org/10.1016/S0304-8853(00)00070-6.
[11] J. Barros, J. Schneider, K. Verbeken, Y. Houbaert, On the correlation between microstructure and magnetic losses in electrical steel, J. Magn. Magn. Mater. 320 (20) (2008) 2490–2493, https://doi.org/10.1016/j.jmmm.2008.04.056.
[12] L. Kestens, S. Jacobs, Texture control during the manufacturing of nonoriented electrical steels, Texture, Stress, Microstruct. 2008 (2008) 1–9, https://doi.org/10.1155/2008/173083.
[13] N. Leuning, S. Steentjes, K. Hameyer, On the homogeneity and isotropy of non-grain oriented electrical steel sheets for the modeling of basic magnetic properties from microstructure and texture, IEEE Trans. Magn. 99 (2017), https://doi.org/10.1109/TMAG.2017.2701508 pp 1–1.
[14] R.M. Bozorth, Ferromagnetism, Van Nostrand, 1951.
[15] G. Bertotti, General properties of power losses in soft ferromagnetic materials, IEEE Trans. Magn. 24 (1) (1988) 621–630, https://doi.org/10.1109/20.43994.
[16] S.E. Zirka, Y.I. Moroz, P. Marketos, A.J. Moses, Loss separation in nonoriented electrical steels, IEEE Trans. Magn. 46 (2) (2010) 286–289, https://doi.org/10.1109/TMAG.2009.2032858.
[17] S.E. Zirka, Y.I. Moroz, P. Marketos, A.J. Moses, Viscosity-based magnetodynamic model of soft magnetic materials, IEEE Trans. Magn. 42 (9) (2006) 2121–2132, https://doi.org/10.1109/TMAG.2006.880685.
[18] G. Bertotti, Hysteresis in Magnetism: For Physicists, Materials Scientists, and Engineers, Gulf Professional Publishing, 1998.

[19] M.F. de Campos, T. Yonamine, M. Fukuhara, F.J.G. Landgraf, C.A. Achete, F.P. Missell, Effect of frequency on the iron losses of 0.5% and 1.5% Si nonoriented electrical steels, IEEE Trans. Magn. 42 (10) (2006) 2812–2814, https://doi.org/10.1109/TMAG.2006.879897.

[20] G. Ban, P.E.D. Nunzio, S. Cicale, T. Belgrand, Identification of microstructure effects in magnetic loss behaviour of 3.2% SiFe NO electrical steels by means of statistical power loss model, IEEE Trans. Magn. 34 (4) (1998) 1174–1176, https://doi.org/10.1109/20.706438.

[21] M. De Wulf, D. Makaveev, L. Dupre, V. Permiakov, J. Melkebeek, Comparison of methods for the determination of dc-magnetic properties of laminated SiFe alloys, J. Appl. Phys. 93 (10) (2003) 8543–8545, https://doi.org/10.1063/1.1557851.

[22] M.F. de Campos, J.C. Teixeira, F.J.G. Landgraf, The optimum grain size for minimizing energy losses in iron, J. Magn. Magn. Mater. 301 (1) (2006) 94–99, https://doi.org/10.1016/j.jmmm.2005.06.014.

[23] K.M. Lee, S.Y. Park, M.Y. Huh, J.S. Kim, O. Engler, Effect of texture and grain size on magnetic flux density and core loss in non-oriented electrical steel containing 3.15% si, J. Magn. Magn. Mater. 354 (2014) 324–332, https://doi.org/10.1016/j.jmmm.2013.11.030.

[24] J. Karthaus, S. Steentjes, N. Leuning, K. Hameyer, Effect of mechanical stress on different iron loss components up to high frequencies and magnetic flux densities, COMPEL – Int. J. Comput. Math. Electr. Electron. Eng. 36 (3) (2017) 580–592, https://doi.org/10.1108/COMPEL-09-2016-0416.

[25] V. Permiakov, L. Dupre, A. Pulnikov, J. Melkebeek, Loss separation and parameters for hysteresis modelling under compressive and tensile stresses, J. Magn. Magn. Mater. 272–276 (Supplement) (2004) E553–E554, https://doi.org/10.1016/j.jmmm.2003.11.381.

[26] N. Leuning, S. Steentjes, M. Schulte, W. Bleck, K. Hameyer, Effect of elastic and plastic tensile mechanical loading on the magnetic properties of NGO electrical steel, J. Magn. Magn. Mater. 417 (2016) 42–48, https://doi.org/10.1016/j.jmmm.2016.05.049.

[27] D. Eggers, S. Steentjes, K. Hameyer, Advanced iron-loss estimation for nonlinear material behavior, IEEE Trans. Magn. 48 (11) (2014) 3021–3024, https://doi.org/10.1109/TMAG.2012.2208944.

[28] S. Jacobs, F. Henrotte, M. Herranz Gracia, K. Hameyer, P. Goes, D. Hectors, Magnetic material optimization for hybrid vehicle PMSM drives, Avere. URLhttp://www.evs24.org/wevajournal/php/download.php?f=vol3/WEVJ3-13960790.pdf.

[29] S. Steentjes, M. Lemann, K. Hameyer, Semi-physical parameter identification for an iron-loss formula allowing loss-separation, Journal of Applied Physics 113 (17) (2013) 17A319, https://doi.org/10.1063/1.4795618 URL http://scitation.aip.org/content/aip/journal/jap/113/17/10.1063/1.4795618.

[30] M. Petrun, S. Steentjes, K. Hameyer, D. Dolinar, 1-d lamination models for calculating the magnetization dynamics in non-oriented soft magnetic steel sheets, IEEE Trans. Magn. 52 (3) (2016) 1–4, https://doi.org/10.1109/TMAG.2015.2480416.28.

[31] M. Petrun, S. Steentjes, K. Hameyer, J. Ritonja, D. Dolinar, Effects of saturation and hysteresis on magnetisation dynamics: Analysis of different material models, COMPEL – Int. J. Comput. Math. Electr. Electron. Eng. 34 (3) (2015) 710–723, https://doi.org/10.1108/COMPEL-10-2014-0286.

[32] B.D. Cullity, C.D. Graham, Introduction to Magnetic Material, 2nd edition, John Wiley & Sons Inc, 2009.